

**GRAPHENE QUANTUM DOTS FROM STYROFOAM
WASTE FOR MULTIDIMENSIONAL APPLICATIONS**

DHEERAJ KUMAR



DEPARTMENT OF TEXTILE & FIBRE ENGINEERING

INDIAN INSTITUTE OF TECHNOLOGY DELHI

JULY 2024

© Indian Institute of Technology Delhi (IITD), New Delhi, 2024

GRAPHENE QUANTUM DOTS FROM STYROFOAM WASTE FOR MULTIDIMENSIONAL APPLICATIONS

by

DHEERAJ KUMAR

Department of Textile & Fibre Engineering

Submitted

in fulfilment of the requirements of the degree of

Doctor of Philosophy

to the



INDIAN INSTITUTE OF TECHNOLOGY DELHI

July 2024

CERTIFICATE

This is to certify that the thesis titled “**Graphene Quantum Dots from Styrofoam Waste for Multidimensional Applications**”, being submitted by **Dheeraj Kumar** to the Indian Institute of Technology Delhi for the award of the degree of **Doctor of Philosophy**, is a record of bonafide research work carried out by him. He has worked under my guidance and fulfilled the requirements for submission of the thesis which has attained the standard required for a Ph.D. degree of this Institute.

The results contained in this thesis have not been submitted, in part or in full, to any other university or institute for the award of any degree or diploma.



Prof. Rajiv K. Srivastava

Department of Textile and Fibre Engineering

Indian Institute of Technology Delhi

New Delhi - 110016, India

Date: 15/07/2024

Place: New Delhi

ACKNOWLEDGEMENTS

I am immensely grateful to Prof. Rajiv K. Srivastava for his invaluable guidance, support, and profound expertise throughout my doctoral journey. His insightful feedback, encouragement, and mentorship have been instrumental in shaping my research and academic development. Prof. Srivastava's dedication to excellence, depth of knowledge, and genuine passion for the subject have inspired me to strive for higher standards and to push the boundaries of my own capabilities. I am deeply indebted to him for his generosity with time, wisdom, and encouragement, which have been indispensable in navigating the challenges of this endeavor. His belief in my potential has been a constant source of motivation, and I am truly fortunate to have had the opportunity to learn from him. I extend my heartfelt gratitude to him for his guidance, mentorship, and unwavering support, which have been integral to the successful completion of this thesis.

I extend my sincere appreciation to the members of my student research committee (SRC) - Prof. Manjeet Jassal, Prof. B. S. Butola, and Prof. B. P. Tripathi, for their helpful contributions to my doctoral journey. Their time-to-time constructive evaluation of my research work, along with their insightful remarks and suggestions, have played a pivotal role in refining the quality and depth of my thesis.


In addition, I express my sincere gratitude to Prof. R. Alagirusamy, the Head of the Department, for his visionary leadership and tireless efforts in continuously upgrading the department with advanced research facilities and improved infrastructure. I would also like to express my heartfelt thanks to all the faculty members and supporting staff of the department for their unwavering support and encouragement throughout my doctoral journey. Special appreciation goes to Mr. Rohit Kumar Chikara, Mr. Rajinder Khatter, Dr. Veerender Sharma, and Mr. Rajkumar Tejanian for their exceptional assistance and support. I am highly grateful to the members of the central research facility (CRF) and nano research

facility (NRF) of IIT Delhi for their prompt and invaluable support in the analysis of samples, which significantly contributed to the success of my research.

It has been an immense pleasure collaborating with my laboratory members, who have not only been exceptional colleagues but also great friends. I am deeply grateful for the all-round support from Dr. Sajan, Dr. Anilkumar, Dr. Avinash, Dr. Sanchayan, Mr. Promod, Ms. Sumana, Mrs. Ekta, Ms. Vanshika, Mr. Aashish, Mr. Advitiya, Ms. Rosemary, Ms. Meenal, Mr. Arvind, and Mr. Sagnik. Their dedication, encouragement, and collective efforts have been invaluable throughout my research journey. Additionally, I would like to express my gratitude to my other friends who provided both scientific and emotional support during my PhD, namely Mr. Peeyush, Mr. Pranay, Ms. Hema, Ms. Jayashree, Ms. Vandana, Mrs. Pratibha, Mrs. Ankita, and Mr. Dinesh Dixit. A special thanks to Mr. Blesson for helping me in various laboratory work. Their friendship and support have been a source of strength and motivation, enriching my experience and contributing to the successful completion of my thesis.

Last but not the least, I express my deepest gratitude towards my beloved mother Mrs. Santosh Devi, my father Mr. Chander Pal, and my family members, Mr. Neeraj, Mrs. Anu, Mrs. Bhavna, and in-laws for their constant support. A special thanks to my beautiful wife Mrs. Sweety Rani and world's sweetest daughter Ms. Dhriti Kuntal for their love in all the ups and downs of my life.

Finally, I thank God for all his blessings!


Dheeraj Kumar

ABSTRACT

Plastic pollution has become a pressing global concern, necessitating innovative solutions for waste management. Among the various forms of plastic waste, Styrofoam® presents a particularly challenging concern due to its high volume, low value, and non-biodegradable nature. Efforts to address this problem have led to the exploration of conventional and advanced methods for converting plastic waste into valuable materials. In this regard, the synthesis of nanomaterials from plastic waste holds significant promise. Nanomaterials offer unique properties and applications, and their synthesis from plastic waste presents a dual benefit of waste management and material valorization. Carbon nanomaterials, in particular, have gained much attention for their versatility and potential applications across diverse fields. Techniques for synthesizing carbon nanomaterials from plastic waste, including both bottom-up and top-down approaches, have been investigated extensively.

In this study, conversion of Styrofoam waste into valorized nanomaterials i.e. graphene quantum dots (GQDs) have been carried out using microwave and hydrothermal pyrolysis and suitability of non-polar and polar GQDs thus synthesized is assessed for advanced applications. Simulation studies were first carried out in understanding and elucidating the mechanism involved in the conversion of Styrofoam to GQDs. Combining simulation methodologies with experimental techniques provided detailed insights for the conversion process of GQDs, facilitating optimization and functionalization strategies. Microwave and hydrothermal pyrolysis methods were selectively explored to synthesis nonpolar and polar GQDs, respectively, from the Styrofoam waste. Morphological and size characterization of GQDs was performed via TEM, while hybridization was confirmed through fringe data and SAED patterns. Functionalities, purity, and yield of GQDs were assessed using XPS and FTIR analyses. GQDs synthesized via microwave pyrolysis were nonpolar in nature, thus adequately soluble in solvents such as toluene and chloroform.

Conversely, GQDs synthesized through hydrothermal method were polar due to presence of hydroxyl, carboxyl, and amine functionalities, as confirmed using XPS, thereby showing solubility in aqueous medium. GQDs exhibited a notably high quantum yield attributed to the phenomenon of multiple excitation generation. Both, microwave and hydrothermal, methods offered efficient and environmentally friendly routes to synthesize GQDs with controlled properties and dimensions.

The synthesized GQDs from Styrofoam waste exhibited remarkable properties that enabled their suitability for application across diverse fields. The GQDs were utilized as coatings, imparting durable hydrophobicity and excellent self-cleaning properties to fabrics. Through the formation of a thin, uniform layer, GQDs effectively repelled water and prevented the adhesion of dirt and stains, thus enhancing the longevity and cleanliness of textiles. Furthermore, GQDs served as crucial components in security ink formulations, offering a solution to combat counterfeit currencies, falsified documents, and tampered goods. GQD-based security inks exhibited high resolution and stability, providing reliable authentication measures for a wide range of applications. In energy storage systems, such as supercapacitors, GQDs played a pivotal role in enhancing capacitance and energy density. When incorporated into electrode materials, GQDs facilitated efficient charge transfer and ion diffusion, resulting in improved electrochemical performance. GQDs-based supercapacitors demonstrated exceptional cycling stability, retaining their capacitive behavior over thousands of charge-discharge cycles. Additionally, GQDs were employed as labeled sensors for metal ion detection, thereby offering selective and sensitive metal ion detection capabilities. Through surface functionalization, GQDs could selectively bind to specific metal ions, leading to distinct changes in their optical or electrical properties. A rapid and accurate detection of metal ions in various environments, including different water sources and industrial processes was thus enabled. Lastly, the development

of an app for on-site detection of colorimetric elements enhanced the practical utility of the technology. A mobile phone based user-friendly platform provided cost-efficient alternative to conventional spectroscopic methodologies, thereby enabling real-time monitoring and analysis across a wide spectrum of materials and surfaces. The synthesis and applications of GQDs synthesized from Styrofoam waste presented a significant advancement not only for plastic waste management but also for the development of advanced nanomaterials for diverse advanced applications.

सारांश

प्लास्टिक प्रदूषण एक वैश्विक चिंता का विषय बन गया है, जिससे अपशिष्ट प्रबंधन के लिए नवीन समाधानों की आवश्यकता है। विभिन्न प्रकार के प्लास्टिक कचरे में से, स्टायरोफोम® एक विशेष रूप से चुनौतीपूर्ण समस्या प्रस्तुत करता है क्योंकि इसका आयतन अधिक होता है, इसका मूल्य कम होता है, और यह गैर-बायोडिग्रेडेबल होता है। इस समस्या के समाधान के प्रयासों ने प्लास्टिक कचरे को मूल्यवान सामग्री में बदलने के पारंपरिक और उन्नत तरीकों के अन्वेषण की दिशा में प्रेरित किया है। इस संदर्भ में, प्लास्टिक कचरे से नैनोमटेरियल्स का संश्लेषण महत्वपूर्ण संभावनाएं रखता है। नैनोमटेरियल्स अद्वितीय गुण और अनुप्रयोग प्रदान करते हैं, और प्लास्टिक कचरे से उनका संश्लेषण अपशिष्ट प्रबंधन और सामग्री मूल्यवर्धन का दोहरा लाभ प्रस्तुत करता है। विशेष रूप से, कार्बन नैनोमटेरियल्स ने अपनी बहुमुखी प्रतिभा और विविध क्षेत्रों में संभावित अनुप्रयोगों के लिए काफी ध्यान आकर्षित किया है। प्लास्टिक कचरे से कार्बन नैनोमटेरियल्स के संश्लेषण के लिए बॉटम-अप और टॉप-डाउन दृष्टिकोणों सहित विभिन्न तकनीकों की व्यापक जांच की गई है।

इस अध्ययन में, स्टायरोफोम कचरे को मूल्यवान नैनोमटेरियल्स, जैसे कि ग्राफीन क्वांटम डॉट्स (जीक्यूडीएस), में बदलने के लिए माइक्रोवेव और हाइड्रोथर्मल पायरोलिसिस का उपयोग किया गया है और इस प्रकार संश्लेषित गैर-ध्रुवीय और ध्रुवीय जीक्यूडीएस की उन्नत अनुप्रयोगों के लिए उपयुक्तता का आकलन किया गया है। स्टायरोफोम को जीक्यूडीएस में बदलने में शामिल तंत्र को समझने और स्पष्ट करने के लिए पहले सिमुलेशन अध्ययन किए गए। सिमुलेशन विधियों को प्रयोगात्मक तकनीकों के साथ मिलाने से जीक्यूडीएस के संश्लेषण की प्रक्रिया के लिए विस्तृत अंतर्दृष्टि मिली, जिससे अनुकूलन और कार्यात्मकरण रणनीतियों की सुविधा मिली। स्टायरोफोम कचरे से गैर-ध्रुवीय और ध्रुवीय जीक्यूडीएस को संश्लेषित करने के लिए क्रमशः माइक्रोवेव और हाइड्रोथर्मल पायरोलिसिस विधियों का चयनित अन्वेषण किया गया। जीक्यूडीएस के रूपात्मक और आकार संबंधी विश्लेषण को ट्रांसमिशन इलेक्ट्रॉन माइक्रोस्कोपी (टीईएम) के माध्यम से किया गया, जबकि हाइड्रिडाइजेशन को फ्रिज डेटा और सिलेक्टेड एरिया इलेक्ट्रॉन डिफ्रेक्शन (एसएईडी) पैटर्न के माध्यम से पुष्टि की गई। जीक्यूडीएस की कार्यक्षमताओं, शुद्धता,

और उपज का आकलन एक्स-रे फोटोइलेक्ट्रॉन स्पेक्ट्रोस्कोपी (एक्सपीएस) और फोरियर ट्रांसफॉर्म इंफ्रारेड (एफटीआईआर) विश्लेषणों का उपयोग करके किया गया। माइक्रोवेव पायरोलिसिस के माध्यम से संश्लेषित जीक्यूडीएस गैर-ध्रुवीय थे, इस प्रकार टोल्यून और क्लोरोफॉर्म जैसे सॉल्वेंट्स में घुलनशील थे। इसके विपरीत, हाइड्रोथर्मल विधि के माध्यम से संश्लेषित जीक्यूडीएस ध्रुवीय थे, क्योंकि उनमें हाइड्रॉक्सिल, कार्बोक्सिल, और अमाइन कार्यात्मकताएं थीं, जैसा कि एक्सपीएस के माध्यम से पुष्टि की गई, इस प्रकार वे जलीय माध्यम में घुलनशील थे। जीक्यूडीएस ने कई उत्तेजना जनरेशन के घटना के कारण उल्लेखनीय रूप से उच्च क्वांटम यील्ड प्रदर्शित की। माइक्रोवेव और हाइड्रोथर्मल दोनों विधियों ने नियंत्रित गुणों और आयामों के साथ जीक्यूडीएस को संश्लेषित करने के लिए कुशल और पर्यावरणीय रूप से अनुकूल मार्ग प्रदान किए।

स्टायरोफोम कचरे से संश्लेषित जीक्यूडीएस ने उल्लेखनीय गुण प्रदर्शित किए, जिन्होंने उन्हें विविध क्षेत्रों में अनुप्रयोग के लिए उपयुक्त बनाया। जीक्यूडीएस का उपयोग कोटिंग्स के रूप में किया गया, जिससे कपड़ों को टिकाऊ हाइड्रोफोबिसिटी और उत्कृष्ट आत्म-सफाई गुण प्राप्त हुए। एक पतली, समान परत के निर्माण के माध्यम से, जीक्यूडीएस ने प्रभावी रूप से पानी को विकर्षित किया और गंदगी और दागों के चिपकने को रोका, जिससे कपड़ों की लंबी उम्र और स्वच्छता बढ़ गई। इसके अलावा, जीक्यूडीएस को सुरक्षा स्याही निर्माण में महत्वपूर्ण घटकों के रूप में उपयोग किया गया, जो नकली मुद्राओं, जाली दस्तावेजों, और छेड़छाड़ किए गए सामानों से लड़ने का समाधान प्रदान करते हैं। जीक्यूडीएस-आधारित सुरक्षा स्याही ने उच्च रिजॉल्यूशन और स्थिरता प्रदर्शित की, जो विभिन्न अनुप्रयोगों के लिए विश्वसनीय प्रमाणीकरण उपाय प्रदान करते हैं। ऊर्जा भंडारण प्रणालियों, जैसे कि सुपरकैपेसिटर में, जीक्यूडीएस ने धारिता और ऊर्जा घनत्व को बढ़ाने में महत्वपूर्ण भूमिका निभाई। इलेक्ट्रोड सामग्री में शामिल होने पर, जीक्यूडीएस ने कुशल चार्ज ट्रांसफर और आयन डिफ्यूजन की सुविधा दी, जिसके परिणामस्वरूप उन्नत इलेक्ट्रोकेमिकल प्रदर्शन हुआ। जीक्यूडीएस-आधारित सुपरकैपेसिटर ने असाधारण साइक्लिंग स्थिरता प्रदर्शित की, अपने धारिता व्यवहार को हजारों चार्ज-डिस्चार्ज चक्रों पर बनाए रखा। इसके अतिरिक्त, जीक्यूडीएस का उपयोग धातु आयन डिटेक्शन के लिए लेबल सेंसर के रूप में किया गया, जिससे चयनात्मक और संवेदनशील धातु आयन

डिटेक्शन क्षमताएं प्राप्त हुईं। सतह कार्यात्मककरण के माध्यम से, जीक्यूडीएस विशिष्ट धातु आयनों से चयनात्मक रूप से बंध सकते थे, जिससे उनके ऑप्टिकल या विद्युत गुणों में विशिष्ट परिवर्तन होते थे। विभिन्न पर्यावरणों, जिसमें विभिन्न जल स्रोत और औद्योगिक प्रक्रियाएं शामिल हैं, में धातु आयनों की तीव्र और सटीक डिटेक्शन को सक्षम किया गया। अंत में, रंगमितीय तत्वों की ऑन-साइट डिटेक्शन के लिए एक ऐप के विकास ने तकनीक की व्यावहारिक उपयोगिता को बढ़ाया। एक मोबाइल फोन आधारित उपयोगकर्ता-मित्र प्लेटफार्म ने पारंपरिक स्पेक्ट्रोस्कोपिक विधियों के लिए एक किफायती विकल्प प्रदान किया, इस प्रकार विभिन्न सामग्रियों और सतहों पर रियल-टाइम मॉनिटरिंग और विश्लेषण को सक्षम किया। स्टायरोफोम कचरे से संश्लेषित जीक्यूडीएस का संश्लेषण और अनुप्रयोग न केवल प्लास्टिक कचरे के प्रबंधन के लिए बल्कि विविध उन्नत अनुप्रयोगों के लिए उन्नत नैनोमटेरियल्स के विकास के लिए एक महत्वपूर्ण प्रगति प्रस्तुत करता है।

Table of Contents

Certificate	i
Acknowledgements	iii
Abstract	v
सारांश	ix
Table of Contents	xiii
List of Figures	xxi
List of Tables	xxvii
List of Symbols	xxix
List of Abbreviations	xxxiii
Chapter 1 Introduction and Motivation	1-24
1.1. Introduction	3
1.2. Motivation	10
1.3. Research objectives	12
1.4. Thesis organization	13
Chapter 2 Theoretical Background and Literature Overview	25-79
2.1. Plastic pollution: looming shadow on tomorrow	27
2.2. Styrofoam waste upcycling	29
2.2.1. Conventional methods	30
2.2.2. Advanced methods	32
2.3. Nanomaterials and their synthesis methods	37
2.3.1. How materials become nanomaterials	37
2.3.2. Nanomaterials synthesis methods	41
2.3.2.1. Playing with individual atoms: Bottom-up	42

2.3.2.2.	Breaking down bulk materials: Top-down	43
2.4.	Carbon nanomaterials from plastic waste	45
2.4.1.	Three-dimensional carbon nanomaterials	45
2.4.2.	Two-dimensional carbon nanomaterials	47
2.4.3.	One-dimensional carbon nanomaterials	49
2.4.4.	Zero-dimensional carbon nanomaterials	50
2.5.	Problems associated with synthesis methods and mechanism	52
2.6.	Zero-dimensional nanomaterial with multi-dimensional applications	54
2.6.1.	Self-cleaning coatings	55
2.6.2.	Security Inks	57
2.6.2.	Supercapacitors	58
2.6.3.	Detectors and sensors	60
2.7.	Summary	62
Chapter 3	Experimental Procedure and Characterization Techniques	81-96
3.1.	Introduction	83
3.2.	Materials	83
3.3.	Methods	84
3.3.1.	Molecular dynamic simulation on synthesis of GQDs	84
3.3.2.	Microwave synthesis of GQDs	84
3.3.3.	Hydrothermal synthesis of GQDs	85
3.4.	Characterization	85
3.4.1.	Transmission electron microscopy	85
3.4.2.	Selected area electron diffraction	86
3.4.3.	UV-Visual spectroscopy	87

3.4.4.	Dynamic light scattering	87
3.4.5.	Raman spectroscopy	88
3.4.6.	Photoluminescence spectroscopy	88
3.4.7.	X-Ray diffraction spectroscopy	89
3.4.8.	Fourier transformation infrared spectroscopy	89
3.4.9.	X-ray photoelectron spectroscopy	90
3.4.10.	Gel permeation chromatography	90
3.4.11.	Nuclear Magnetic Resonance	91
3.4.12.	Thermogravimetry analysis	91
3.4.13.	Contact angle goniometer	92
3.4.14.	Brunauer-Emmett-Teller (BET) surface area	92
3.4.15.	Potentiostat/Galvanostat	93
3.4.16.	Ultraviolet (UV) chamber	93
3.4.17.	RGBGr (red, green, blue, gray) analysis	94
3.4.18.	Web-app programming language	94
3.4.19.	Large-scale atomic/molecular massively parallel simulator (LAMMPS)	95
Chapter 4	Molecular Dynamics Investigation for GQD Synthesis from Styrofoam Waste	97-118
4.1.	Introduction	99
4.2.	Experimental	101
4.2.1.	Materials	101
4.2.2.	Methods	101
4.2.2.1.	Simulation setup	101
4.2.2.2.	Simulation experiments	102

4.2.2.2.	Simulation script	104
4.2.3.	Characterization and software	105
4.2.3.1.	Thermogravimetry analysis	106
4.2.3.2.	Nuclear Magnetic Resonance	106
4.2.3.3.	Large-scale atomic/molecular massively parallel simulator (LAMMPS)	106
4.2.3.4.	Ovito	107
4.2.3.5.	Blender	107
4.3.	Results and Discussion	108
4.3.1.	Evolution of cyclic structure from polystyrene	108
4.3.2.	Formation of GQDs from cyclic structure	111
4.4.	Conclusion	113
Chapter 5	Green Synthesis of Nonpolar GQDs from Styrofoam Waste	119-138
5.1.	Introduction	121
5.2.	Experimental	124
5.2.1.	Materials	124
5.2.2.	Methods	124
5.2.2.1.	Nonpolar GQDs synthesis from Styrofoam waste via microwave method	124
5.2.3.	Characterization and equipment	125
5.2.3.1.	Microwave furnace	125
5.2.3.2.	Gel permeation chromatography	125
5.2.3.3.	Transmission electron microscopy	125
5.2.3.4.	SAED calculations	126
5.2.3.5.	Raman spectroscopy	126

5.2.3.6.	Photoluminescence spectroscopy	126
5.2.3.7.	Fourier transformation infrared spectroscopy	127
5.2.3.8.	X-Ray diffraction spectroscopy	127
5.2.3.9.	X-ray photoelectron spectroscopy	127
5.3.	Results and Discussion	127
5.4.	Conclusion	134
Chapter 6	Multifaceted Applications of Nonpolar QDs	139-182
6.1.	Introduction	141
6.2.	Experimental	147
6.2.1.	Materials	147
6.2.2.	Methods	148
6.2.2.1.	Preparation of QDs coated cotton fabric	148
6.2.2.2.	QDs based printer cartridge preparation	149
6.2.2.3.	Preparation of carbonized electrospun PAN matrix	149
6.2.2.4.	Fabrication of three- and two-electrodes based supercapacitor	150
6.2.3.	Characterization	152
6.2.3.1.	Contact angle goniometer	152
6.2.3.2.	Ultraviolet (UV) chamber	152
6.2.3.3.	Transmission electron microscopy	152
6.2.3.4.	Raman spectroscopy	152
6.2.3.5.	X-ray photoelectron spectroscopy	153
6.2.3.6.	Brunauer-Emmett-Teller (BET) surface area	153
6.2.3.7.	Potentiostat/Galvanostat	153

6.2.3.8.	Area capacitance calculation	154
6.3.	Results and Discussion	154
6.3.1	Hydrophobic GQDs coating for self-cleaning	154
6.3.2.	GQDs based security ink	156
6.3.3.	GQDs as active material for supercapacitor	158
6.3.3.1.	Three-electrode electrochemical studies	162
6.3.3.2.	Two-electrode electrochemical studies	169
6.4.	Conclusion	172
Chapter 7	Synthesis of Polar GQDs for Selective Metal Ion Detection	183-207
7.1.	Introduction	185
7.2.	Experimental	187
7.2.1.	Materials	187
7.2.2.	Methods	188
7.2.2.1.	Polar GQDs synthesis from Styrofoam waste via hydrothermal method	188
7.2.3.	Characterization and equipment	189
7.2.3.1.	Transmission electron microscopy	189
7.2.3.2.	Dynamic light scattering spectroscopy	189
7.2.3.3.	Raman spectroscopy	189
7.2.3.4.	Photoluminescence spectroscopy	189
7.2.3.5.	UV-Visual spectroscopy	190
7.2.3.6.	Quantum yield calculation	190
7.2.3.7.	X-ray photoelectron spectroscopy	191
7.2.3.8.	RGBGr (red, green, blue, gray) analysis	191
7.3.	Results and Discussion	191

7.3.1. Properties of GQDs	191
7.3.2. Copper ion detection	198
7.4. Conclusion	203
Chapter 8 On-Site App-based Detection of Colorimetric Elements	209-235
8.1. Introduction	211
8.2. Experimental	213
8.2.1. Materials	213
8.2.2. Working principle	213
8.2.3. Methods	214
8.2.3.1. Preparation of reference sticker	214
8.2.3.2. Preparation of colorimetric samples	215
8.2.3.3. App development code	216
8.2.3.3.1. JavaScript Code	216
8.2.3.3.2. HTML Code	219
8.2.3.3.3. CSS Code	222
8.2.4. Characterization and programming language	226
8.2.4.1. RGBGr (red, green, blue, gray) analysis	226
8.2.4.2. Web-app programming language	227
8.3. Results and Discussion	228
8.4. Conclusion	233
Chapter 9 Conclusions and Future Outlook	237-241
9.1. Conclusions	239
9.2. Future Outlook	240
<i>Curriculum Vitae</i>	243

List of Figures	Page
Figure 1.1 Integrated circular economy approach: Upcycling plastic waste into GQDs for multidimensional applications.	12
Figure 2.1 Conventional methods for plastic waste recycling and their related problems: from mechanical grinding to thermal treatment for producing household items.	31
Figure 2.2 Advanced methods for plastic waste recycling and their related problems: hydrogenolysis, gasification and bioconversion for advanced applications.	33
Figure 2.3 Concept of quantum confinement in nanoparticles.	40
Figure 2.4 Top-down and bottom-up approaches in nanomaterial synthesis.	41
Figure 2.5 Methodology and limitations: Biodegradable waste conversion to GQDs via carbonization followed by acid/base treatment.	51
Figure 4.1 (A) NMR and (B) TGA of waste Styrofoam performed to determine tacticity and degradation temperature, respectively.	103
Figure 4.2 Three-dimensional model of polystyrene molecule with (A) three and (B) five degrees of polymerization.	108
Figure 4.3 (A) Polystyrene molecule degradation into cyclic ring structure (shown in red color) without hydrogen atoms. (B) Different cyclic ring structures formed by changing the random number associated with velocity.	109
Figure 4.4 (A) Cyclic structures taken in simulation box with hydrogen atoms. (B) GQDs structure formation after the simulation from cyclic structure with hydrogen atoms.	110

Figure 4.5 (A) Cyclic structures taken in simulation box without hydrogen atoms. (B) GQDs structure formation after the simulation from cyclic structure without hydrogen atoms.	111
Figure 4.6 GQDs formation, presence of cyclic structure, and formation of intermediate species with respect to time from cyclic structure (A) with and (B) without hydrogen atoms.	112
Figure 4.7 Proposed synthesis mechanism of GQDs based on simulation study.	113
Figure 5.1 (A) and (B) representative TEM images of the sample, SAED and particle size distribution graph is inserted in (B) at top right and left corners respectively. (C) Gray scale fringe data profile inserted on high resolution TEM image. (D) Raman spectrum of GQDs.	128
Figure 5.2 (A) Photoluminescence spectrum of GQD sample, inserted image - excitation in a UV chamber. (B) GQD yield calculated at varying exposure time and temperature from FTIR spectra.	129
Figure 5.3 (A), (B) and (C) FTIR spectra of synthesized GQDs depending upon temperature (in the range of 270-390 °C) and exposure time (0-30 minutes) dissolved in chloroform. (D) FTIR spectra of waste Styrofoam dissolved in chloroform at different concentrations. All the spectra were performed in KBr liquid cell.	131
Figure 5.4 (A) XRD spectrum of GQD sample. (B) XPS full scan survey, and high resolution C1s spectrum is inserted at top right corner.	133
Figure 6.1 Preparation of nonpolar GQDs coated cotton fabric for self-cleaning application.	148
Figure 6.2 Preparation of nonpolar GQDs based printer cartridge for security ink application.	149

Figure 6.3 Schematic of (A) three-electrode and (B) two-electrode electrochemical cell fabrication system.	151
Figure 6.4 Self-cleaning behavior of (A) pristine and (B) GQD coated cotton fabric.	155
Figure 6.5 (A) Absorption of tea, coffee, milk, and juice on pristine and GQD coated cotton fabric. (B) Contact angle measurements of coated fabric after washing with water and surfactant.	156
Figure 6.6 GQDs image taken in (A) white light showing light yellow color and (B) showing green color in UV light.	157
Figure 6.7 GQDs based secured ink printed on a white paper (A) under normal light (B) under UV light.	158
Figure 6.8 (A) TEM image of cPAN fibres. (B) 0.4 mg GQDs coated cPAN fibres and high-resolution image of GQDs inserted on the top left corner.	159
Figure 6.9 XPS full scan survey of (A) neat cPAN and (B) 0.4 mg GQDs coated cPAN fabric (Highly resolution C1s spectrum is inserted at the top-right corner).	160
Figure 6.10 Raman spectra of (A) neat cPAN and (B) 0.4 mg GQDs coated cPAN fibre.	161
Figure 6.11 Contact angle measurement of (A) neat cPAN fibre (137°) and (B) GQDs coated cPAN (145°). (C) BET of neat cPAN and GQDs coated cPAN fibre.	161
Figure 6.12 (A) CV curves collected for neat cPAN and different concentration of GQDs coated cPAN at 100 mVs ⁻¹ scan rate. CV curves of (B) 0.4 mg and (C) 0.1 mg GQDs coated cPAN matrices collected under various scan rates. (B) GCD curves collected for neat cPAN and 0.1 mg GQDs coated cPAN matrices	163

Figure 6.13 | (A) GCD curves of 0.1 mg GQDs coated cPAN matrices collected under various current densities. (B) Specific capacitance of neat and GQDs coated cPAN matrices at different current densities. 166

Figure 6.14 | (A) Nyquist plot of GQDs coated cPAN matrix with circuit fit and circuit diagram inserted on the lower right-hand side. (B) Ragone plot of energy density and power density for neat and GQDs coated cPAN matrices. 167

Figure 6.15 | (A) Three-electrode system areal capacitance, energy density and power density literature survey [82]-[91] as compared with 0.4 mg and 0.1 mg GQDs coated cPAN electrode. (B) The literature survey of areal capacitance, energy density and power density of two-electrode system [92]-[103] as compared to fabricated coin cell. 168

Figure 6.16 | (A) CV curves of 0.1 mg GQDs coated cPAN matrices collected under various scan rates. (B) CV curves of neat cPAN and 0.1 mg GQDs coated cPAN matrices collected with three- and two-electrode system-based supercapacitor. Two-electrode system (C) GCD curves of 0.1 mg GQDs coated cPAN matrices collected under various current densities. (D) Two-electrode Nyquist plot of 0.1 mg GQDs coated cPAN matrices with circuit fit and circuit diagram inserted at top center. 169

Figure 6.17 | (A) 0.1 mg GQDs coated cPAN matrix capacitance retention for 3000 cycles in two-electrode supercapacitor. (B) Ragone plot of energy density and power density 0.1 mg GQDs coated two-electrode system. 171

Figure 7.1 | (A) High resolution TEM images showing nanoscale morphology of GQDs sample and (B) fringes of GQDs sample. (C) Grayscale profile generated using ImageJ for the calculation of d spacing. (D) DLS elucidating size distribution and uniformity of GQDs in solution. 192

Figure 7.2 (A) Raman spectra depicting vibrational modes of the synthesized GQDs sample. (B) ID/IG ratio graph illustrating the relationship between GQDs sample with different reaction conditions and their ID/IG ratio.	193
Figure 7.3 Figure 3 (A) XPS analysis detailing the structural characteristics and electronic states of synthesized GQDs. High-resolution (B) C1s, (C) N1s, and (D) O1s spectra providing in-depth insights into the sp ² hybridization structure, nitrogen functionalities, and oxygen functionalities, respectively.	194
Figure 7.4 (A) UV-Vis spectra capturing the electronic absorption characteristics of various GQDs samples. (B) PL spectra revealing the luminescent behavior of GQD samples, both instrumental in the calculation of quantum yield.	197
Figure 7.5 (A) Twenty different metal salts. (B) Color change observed after adding GQDs to the metal salt solutions.	198
Figure 7.6 (A) Copper (II) salts. (B) Color change observed after adding GQDs. (C) Copper (I) salts. (D) Color change observed after adding GQDs.	199
Figure 7.7 Copper (II) salt in different environments, (A) tap water, (B) Ganga water, (C) acidic water, and (D) basic water and their respective color changes observed after adding GQDs.	200
Figure 7.8 (A) Green color of known concentration copper (II) in water after adding GQDs. (B) Green color of unknown samples under similar conditions.	201
Figure 7.9 (A) Calculated red, green, blue, and gray intensities of green color copper (II) samples shown in figure 8A. (B) Linear fit data of gray color intensity versus concentration and linear fit parameters are inserted into top right corner. (C) UV-Vis spectroscopy of known and unknown concentration copper (II) in water after adding GQDs. (D) Known sample absorbance versus concentration	202

plot with linear fit data. Equation and linear fit parameters inserted in the bottom right corner of the graph.

Figure 8.1 | Illustration of the operational mechanism of the developed application. 214

Figure 8.2 | Plastic transparent cuvette with (A) RGB reference sticker on the front side and (B) white sticker on the back side when lights are on. 215

Figure 8.3 | (A) Basic user interface of the developed app. Setting the (B) reference sticker color and (C) sample color in the app to determine the concentration of unknown calorimetric compound. 227

Figure 8.4 | Solution of calorimetric compound (copper acetate) with known concentrations from 0.1 to 0.0025 molar. 228

Figure 8.5 | (A) Calibration graph plotted between RGBGr intensity and concentration on solution. (B) linear fitting performed on red intensity and concentration of solution. 230

Figure 8.6 | Solution of calorimetric compound (copper acetate) with concentrations (A) 0.06 M, (B) 0.02 M and (C) 0.006 M in normal light condition, which needs to be calculated using the app. 231

Figure 8.7 | Solution of calorimetric compound (copper acetate) with concentrations (A) 0.06 M and (B) 0.02 M in lower light condition, which needs to be calculated using the app. 232

List of Tables	Page
Table 5.1 FTIR peak (2926 cm ⁻¹) height table for different concentrations of Styrofoam.	130
Table 5.2 Yield and purity calculations performed using FTIR results.	131
Table 6.1 Areal and volumetric capacitance of neat cPAN based three-electrode system at varying current density values.	164
Table 6.2 Areal and volumetric capacitance of 0.1 mg GQDs coated cPAN based three-electrode system at varying current density values.	165
Table 6.3 Areal and volumetric capacitance of 0.4 mg GQDs coated cPAN based three-electrode system at varying current density values.	166
Table 6.4 Areal and volumetric capacitance of 0.1 mg GQDs coated cPAN based two-electrode system at varying current density values.	170
Table 7.1 GQDs synthesis parameters, encompassing quantities of Styrofoam, acetone, ammonia, hydrogen peroxide, reaction temperature, and duration.	188
Table 7.2 Quantum yield calculated for all samples based on UV-Vis and PL spectroscopy.	190
Table 7.3 Percentage of carbon, nitrogen, and oxygen determined through XPS analysis for all GQD samples.	196
Table 8.1 Average RGBGr values calculated from 0.1 to 0.0025 molar concentration.	229
Table 8.2 Average RGBGr values calculated for unknown samples in normal light condition.	231
Table 8.3 Average RGBGr values calculated for unknown samples in lower light condition.	232

List of Symbols

®	Registered trademark symbol
%	Percentage
°	Degrees
±	Plus, or minus
50X	50 times
2θ	2 times theta
δ	Delta
nm	Nanometers
mm	Millimeters
cm	Centimeters
cm ⁻¹	Centimeters inverse
cm ²	Centimeters square
°C	Degrees Celsius
K	Kelvin
s	Seconds
min	Minutes
fs	Femtoseconds
ns	Nanoseconds
ps	Picoseconds
°C/min	Degrees Celsius per minute
scans/min	Scans per minute
g	Grams
mg	Milligrams

mL	Milliliters
μL	Microliters
mL/hr	Milliliters per hour
eV	Electron volts
M	Molar
M_w	Weight-average molecular weight
M_n	Number- average molecular weight
M_z	Z-average molecular weight
M_p	Peak molecular weight
g/mol	Grams per mole
I	Current
C	Capacitance
V	Volts
E	Energy
t	Time
mV	Millivolts
mW	Milliwatts
Ω	Ohms
Hz	Hertz
GHz	Gigahertz
kHz	Kilohertz
kW	Kilowatts
kWh	Kilowatt-hours
Δt (s)	Change in time in seconds
ΔV (V)	Change in potential in volts

mAcm^{-2}	Milliamperes per square centimeter
mFcm^{-2}	Millifarads per square centimeter
Fg^{-1}	Farads per gram
μWhcm^{-2}	Microwatt-hours per square centimeter
μWcm^{-2}	Microwatts per square centimeter
mVs^{-1}	Millivolts per second
$\text{Re}(z)/\text{Ohm}$	Real part of impedance per Ohm
$-\text{Im}(Z)/\text{Ohm}$	Negative imaginary part of impedance per Ohm
ϕ_s	Quantum yield of sample
ϕ_r	Quantum yield of reference
PL_r	Photoluminescence of reference
PL_s	Photoluminescence of sample
UV_s	Ultraviolet spectrum of sample
UV_r	Ultraviolet spectrum of reference
η_s	Refractive index of sample
η_r	Refractive index of reference
p/p_0	Pressure ratio
$p/V(p_0-p)$	Pressure-volume ratio
Cu^{1+}	Cuprous ion
Cu^{2+}	Cupric ion
MgO	Magnesium oxide
$\text{Mg}(\text{OH})_2$	Magnesium hydroxide
Fe	Iron
KOH	Potassium hydroxide
KOAc	Potassium acetate

H_2SO_4	Sulfuric acid
ZnCl_2	Zinc chloride
TiO_2	Titanium dioxide
H_2O_2	Hydrogen peroxide
Hg	Mercury
Hg^{2+}	Mercuric ion
Cu	Copper
Ag	Silver
AgCl	Silver chloride
KCl	Potassium chloride
Pb	Lead
Pb^{2+}	Lead ion
CdTe	Cadmium telluride
CdS	Cadmium sulfide
CDCl_3	Deuterated chloroform
C-O	Carbon-oxygen bond
C=O	Carbon-double bond oxygen
C-N	Carbon-nitrogen bond
C=C	Carbon-double bond carbon
C-C	Carbon-carbon bond
C-NH ₂	Amino group attached to carbon

List of Abbreviations

1D	One dimensional
2D	Two dimensional
3D	Three dimensional
MW	Microwave
USD	United States dollar
NNI	National nanotechnology initiative
USEPA	United States environmental protection agency
PC	Personal computer
HTML	Hypertext markup language
CSS	Cascading style sheets
a.u.	Arbitrary units
Conc.	Concentration
sols	Solutions
RGB	Red, green, and blue
RGBGr	Red, green, blue, and gray
QDs	Quantum dots
GQDs	Graphene quantum dots
CQDs	Carbon quantum dots
GO	Graphene oxide
SDS	Sodium dodecyl sulfate
PVC	Polyvinyl chloride
LDPE	Low-density polyethylene
PU	Polyurethane

PS	Polystyrene
PET	Polyethylene terephthalate
THF	Tetrahydrofuran
cPAN	Carbonized polyacrylonitrile
CNTs	Carbon nanotubes
CNS	Carbon nanosheets
DNA	Deoxyribonucleic acid
MOFs	Metal-organic frameworks
UV	Ultraviolet
UV-Vis	Ultraviolet-Visible
TEM	Transmission electron microscopy
SAED	Selected area electron diffraction
DLS	Dynamic light scattering
PL	Photoluminescence
XRD	X-ray diffraction
FTIR	Fourier transform infrared
XPS	X-ray photoelectron spectroscopy
NMR	Nuclear magnetic resonance
TGA	Thermogravimetric analysis
GC-MS	Gas chromatography-mass spectroscopy
BET	Brunauer-Emmett-Teller
AAS	Atomic absorption spectroscopy
ICP-AES	Inductively coupled plasma atomic emission spectroscopy
ICP-MS	Inductively coupled plasma mass spectroscopy
GPC	Gel permeation chromatography

OCA	Optical contact angle
ID/IG	Intensity of defect band / intensity of graphitic band
CVD	Chemical vapor deposition
DP	Degrees of polymerizations
GCD	Galvanostatic charge–discharge
EIS	Electrochemical impedance spectroscopy
Rs	Series resistance
Rct	Charge transfer resistance
EDL	Electrochemical double-layer
EDLCs	Electrochemical double-layer capacitors
MD	Molecular dynamics
ReaxFF	Reactive force field
LAMMPS	Large-scale atomic/molecular massively parallel simulator
.traj	Trajectory
NVT	Number, volume, and temperature